doi.org/10.1002/ejic.202100304

Unraveling All-Inorganic $CsPbI_3$ and $CsPbI_2Br$ Perovskite Thin Films Formation – Black Phase Stabilization by $Cs_2PbCl_2I_2$ Addition and Flash-Annealing

Edouard Breniaux,[a] Pascal Dufour,[b] Sophie Guillemet-Fritsch,[c] and Christophe Tenailleau*[c]

Phase formation and transformation of 3D inorganic halide perovskites $CsPbI_3$ and $CsPbI_2Br$ were investigated by in-situ X-ray diffraction (XRD) in nitrogen or air from 30 °C up to 320 °C. Thin films were obtained by spin-coating of a liquid solution of salt precursors dissolved in DMSO under normal conditions. XRD data analysis, by using the Le Bail method, evidenced for the first time, to our knowledge, the spontaneous crystallization of black orthorhombic γ phase at ambient temperature, for both 3D perovskite phases. For once, this black γ phase could be studied upon heating. It transforms to the black tetragonal β and cubic α phases. The reverse transitions were also evidenced upon cooling. The influence of the all-inorganic 2D $Cs_2PbI_2Cl_2$ material addition over the black phase stability was unprecedently analyzed by in-situ XRD. The mixture of the 3D and 2D phases, or mix [3D + 2D], exhibits an improved stability of the black phase compared to the single 3D phase, and tends to induce highly oriented thin films and increased compactness, probably due to chemical insertion or anchoring. Finally, flash-annealed thin films at various temperatures (RT < T < 325 °C) of $CsPbI_2Br$ in air, alone and in the presence of the 2D phase, were studied. A more textured layer is evidenced for the mix [3D + 2D] thin film, showing larger grains and more compact films above 200 °C. The mix [3D + 2D] film flash-annealed at 300 °C remained black for four days after air exposure and 50% relative humidity.

Introduction

The impressive properties of perovskite materials provide a good solution to improve new and old silicon-based solar panels with tandem technology, which already reached more than 29% efficiency in 2020. Perovskite solar cells are on their way to industrialization with large breakthroughs to come in the use of photovoltaic technologies for portable electronic devices, transports and building-integrated systems. The hybrid (organic-inorganic) lead halide perovskites, such as $MAPbI_3$ or MAPI (E_g ~ 1.6 eV) and $FAPbI_3$ or FAPI (E_g ~ 1.5 eV) (with MA for Methylammonium and FA for Formamidinium), present the best efficiencies and can challenge single-crystal silicon, but it still suffers from instability in air. Therefore, lead reduction and stability are the last hindrances to overcome for perovskite to be on our buildings and transportable systems. All-inorganic perovskite solar cells, including the reference material $CsPbI_3$ (E_g ~ 1.7 eV), have shown continuous increased performances over the last couple of years reaching more than 18% efficiency in 2018, and more than 20% in 2021 with an MACl sequential dripping solution.[1,2] Such systems, avoiding the use of volatile and hydrophilic organic cations, have become more and more interesting for photovoltaic applications, as well as for lasers, LEDs or photodetectors.[1,3,4] Fully inorganic materials are usually more stable than their hybrid counterpart but most of the performing inorganic perovskites remain quickly degradable in ambient atmosphere, mainly due to water penetration. Indeed, moisture environment usually drives to the formation of an undesired yellow phase, known as the delta $CsPbI_3$ phase, which crystallizes in a non-perovskite structure composed of disconnected octahedra and exhibits a higher bandgap of ~ 2.8 eV.[5,6] There are many ways to overcome stability issues: (i) by substitution on the *A* and/or *B* site of the ABX_3 perovskite-type (*X*=Cl, Br, I) or interstitial insertion, (ii) insertion of organic spacers for 2D-type structures, (iii) surface passivation by additives, or (iv) device encapsulation.[7,8] In the ideal form, the crystal structure of cubic ABX_3 perovskite can be described by corner sharing [BX_6] octahedra with the *A* cation occupying a 12-fold coordination site.

In 2018, Marronnier et al. confirmed what Trots and Myagokta characterized 10 years earlier upon heating of the yellow orthorhombic delta phase of $CsPbI_3$ powders introduced in air sealed quartz capillaries.[9,10] It transforms into a black cubic alpha phase above 314 °C. Thanks to high-resolution in-

[a] *E. Breniaux*
Université de Toulouse
CIRIMAT, CNRS
Toulouse, France
E-mail: breniaux@chimie.ups-tlse.fr
[b] *Prof. Dr. P. Dufour*
Université de Toulouse
CIRIMAT, CNRS
Toulouse, France
E-mail: dufour@chimie.ups-tlse.fr
[c] *S. Guillemet-Fritsch, Prof. Dr. C. Tenailleau*
Université de Toulouse
CIRIMAT, CNRS
Toulouse, France
E-mail: tenailleau@chimie.ups-tlse.fr

Supporting information for this article is available on the WWW under https://doi.org/10.1002/ejic.202100304

Part of the joint "Perovskite Materials and Devices" Special Collection with ChemPlusChem.

situ synchrotron X-Ray Diffraction (XRD) measurements, Marronnier and coworkers also showed that the cubic phase starts to transform into a black tetragonal beta phase at 280 °C upon cooling. At 180 °C a black orthorhombic gamma phase is crystallized, that can remain as a metastable perovskite polytype for a few days once cooled down to RT, which is still very important for photovoltaic applications. Further information of the crystal structure of the metastable black phase of $CsPbI_3$ was revealed by Sutton et al. in 2018 by using theory and experimental works.[11] In their article, they clearly challenged the assumptions made by some authors to have been able to trap the cubic alpha phase at room temperature. They demonstrate that after heating powders or thin films of the yellow $CsPbI_3$ material formed in nitrogen atmosphere, the black orthorhombic gamma phase is obtained straight back after cooling down to room temperature, which ultimately transforms again into the yellow non-perovskite delta phase after a short period of time. An additive such as concentrate aqueous hydriodic acid (HI) can be used to facilitate formation of black thin layers at low temperatures, although Ke et al. evidenced for the formation of a black hybrid $Cs_{1-x}DMA_xPbI_3$ phase (with DMA = dimethylamine) following the HI induced decomposition of dimethylformamide (DMF).[12]

The black phase stabilization is a primarily issue for the use of inorganic solar cells. Steele et al. also reported the use of substrate clamping and biaxial strain to provide stability to black phase $CsPbI_3$ thin films at room temperature after heating.[13] Some papers claim to have stabilized the cubic alpha phase at room temperature by doping or addition of a second component while XRD patterns sometimes evidence for a splitting of some (hkl) planes or extra peaks which then clearly indicate a lower symmetry. Therefore, caution should be taken about the nature of the phase obtained each time and research needs to be pushed further in order to ensure that the fabrication process of each material is understood. Also, to the best of our knowledge, the black phase is usually only discussed in $CsPbI_3$ after a first heating stage of the pristine material, in particular for thin films. In 2020, Nasström et al. presented the phase diagram of $CsPb(Br_xI_{1-x})_3$ from room temperature (RT) up to 312 °C.[14] Precursors solutions mixed with dimethyl sulfoxide (DMSO) in nitrogen atmosphere were ink-printed as thin films and annealed at 60 °C. Samples were then exposed to a humid environment in order to obtain the most stable phase at RT and analyzed by grazing incidence wide angle x-ray spectroscopy (GIWAXS) in an air-tight heating chamber flushed with nitrogen. They showed that the metastable perovskite is stabilized in their films upon cooling down in the presence of bromide and that the transition temperatures monotonically decrease with increasing bromide concentration.

$CsPbI_2Br$ ($E_g \sim 1.9$ eV) is more stable than $CsPbI_3$ in ambient conditions, the latter being thus generally processed under nitrogen conditions to minimize the yellow phase. Preparation of such phase at low temperature is already well studied in the literature.[15,16] Understanding the thermal behavior of $CsPbI_2Br$ and stabilizing its black phase would also be an interesting opportunity to facilitate its use for photovoltaic devices. Using organic spacers to stabilize inorganic phases is largely studied,[17–20] but usually brings back the problem of thermal stability of such organic molecules and can decrease electronic conduction properties through thermodynamic barriers. Li et al. have recently prepared a new halide phase of lower dimensionality, namely $Cs_2PbI_2Cl_2$.[21] This inorganic 2D phase of Ruddlesden-Popper structural type is stable in air and at high temperature (T ~ 400 °C), with a higher band gap ($E_g \sim 3.0$ eV) and shows photoconductivity. During our research investigations on the doping and use of the 2D $Cs_2PbCl_2I_2$ phase, we have recently noticed that mixing a 2D inorganic material with a 3D inorganic perovskite could keep the black phase for longer than usual after heating.[22] This observation was confirmed by Li. et al. who published only a few months ago their results on the stabilization of mixed dimensional fully inorganic perovskite-based solar cells with enhanced efficiency.[23,24] Elsewhere, it has been showed that a 3D $CsPbI_2Br$ phase encapsulated in between layers of 2D $Cs_2PbCl_2I_2$ nano-sheets is far more stable in ambient conditions than the 3D material alone and the efficiency of such heterostructure can reach up to 16.6 %.[25] The good stability of the 2D phase against humidity and temperature, which can passivate the perovskite surface, increase hydrophobicity, hamper moisture reaction and change the film morphology is also essential for optoelectronic applications.[26–28]

In this paper, we present a systematic study of the $CsPbI_3$ and $CsPbI_2Br$ perovskite phases formed from a liquid solution at room temperature and just after spin-coating in air. Our study shows for the first time that the perovskite solution crystallizes spontaneously under its gamma black phase, straight after spin-coating. Phase transformation was then analyzed upon heating and cooling by in-situ XRD measurements. In the first part of the results, a thin layer of 3D phases ($CsPbI_3$ or $CsPbI_2Br$) was characterized in nitrogen atmosphere. The black phase obtained at room temperature is clearly identified as an orthorhombic phase. Therefore, we challenge other previous studies that identified it as the cubic phase, probably due to texture effects after thermal treatments. In the second part, a mixture of the 3D phase ($CsPbI_3$ and $CsPbI_2Br$) mixed with the 2D material ($Cs_2PbI_2Cl_2$) was probed, still in nitrogen, and the effects of the 2D addition over the film structure and texture were characterized. We show that a 2D phase additive can greatly improve the 3D phase stability, even for the very unstable $CsPbI_3$ black phase, and allows to keep it back to room temperature after heating. A slowdown of crystallization and textured films are observed for the mixture. In the third part, 3D $CsPbI_2Br$ and mix [3D $CsPbI_2Br$ + 2D] thin films were analyzed by in-situ XRD performed in air. In the fourth part, air flash-annealed thin films of 3D $CsPbI_2Br$ and mix [3D $CsPbI_2Br$ + 2D] were studied by XRD and the film surface morphology was characterized by scanning secondary electron microscopy (SEM). Finally, thermal expansion coefficient and strain parameter ε are evidenced to be lower for the mix [3D + 2D], which explains how the 2D phase stabilizes the black phase after crystallization, reducing and influence the resulting strain in the film.

Results and Discussion

In-situ XRD analysis of 3D inorganic halide perovskites under nitrogen atmosphere

3D $CsPbI_3$ thin films

XRD is a conventional and powerful technique to characterize crystalline materials. The phase formation and transformation results obtained on the very promising all-inorganic 3D halide perovskite material for photovoltaics, so-called reference $CsPbI_3$ sample, are presented first and discussed in this part. Freshly spin-coated perovskite thin films were put straight in the XRD chamber to observe spontaneous crystallization, and were further analyzed upon heating to study crystalline structure variations. The outline of this handling is represented in Figure 1a. Generally, the crystalline delta phase can easily be characterized by a first split peak at 9.9° in 2-Theta corresponding to the (011) and (002) planes of the non-perovskite yellow phase and a main peak for polycrystalline materials at 26.5° assigned to the (122) series. The different XRD patterns of $CsPbI_3$ polymorphs are represented in Figure S1 with the corresponding planes attributed to diffraction peaks. A minimum of ~2 wt% of crystalline phase can usually be evidenced on our XRD patterns. The delta phase appears a few minutes only after spin-coating and XRD analysis performed in air within 16 minutes. Its behavior upon heating and cooling has already been presented elsewhere.[9] But if we put $CsPbI_3$ thin films under nitrogen gas in the XRD chamber straight after spin coating in air, a single black phase is observed at 30 °C (see Figure 2a). Indeed, two main sets of peaks appear at ~14.4° and more intensively at ~28.8° in 2-Theta. None are observed at the usual 2-Theta values that correspond to the delta phase. As a reminder, there was no additive used during the synthetic procedure based on the mixture of the cesium and lead iodide precursors in DMSO, while the following spin-coating procedure was operated in air conditions. This corresponds already to a great novelty as it is shown here that the gamma phase of $CsPbI_3$ can form spontaneously at ambient temperature. Pattern matching mode was used to identify the phase symmetry and to refine the cell parameters (see Figure 2b and Figure 3a). Error bars, taken out from the Fullprof calculation file, are always included in the symbol size. ITO layer underneath our spin-coated film was used to check for any sample shift. The XRD pattern can be fully indexed with an orthorhombic *Pnam* space group and $a = 8.853(3)$, $b = 8.588(3)$ *and* $c = 12.477(1)$ Å, matching very well the results obtained by Sutton et al. for the black orthorhombic gamma phase obtained after heat treatment of $CsPbI_3$ and cooling.[11] Marronnier et al. calculated a lower free energy for the gamma phase than for the delta phase.[9] Here, we experimentally confirm the spontaneous perovskite crystallization from a DMSO solution to the gamma phase. Let us also mention here that these last authors used the *Pbnm* space group to describe earlier the same phase, which would simply correspond to an axis inversion in comparison to Sutton.[9] In the following, our data will be presented based on Sutton's description. The split peaks at ~14.4 and 28.8° correspond to the (002)/(110), and (004)/(220) planes, respectively. A higher intensity on the second sets of (hkl) planes can suggest that the film is crystallizing as the XRD pattern is being recorded with preferred orientations along those two directions. Preferred orientation along $<002>$ and $<110>$ directions was also observed for 3D MAPI and MAP(I,Cl) films.[29] They showed that adding $CsPbBr_3$ to MAPI can change the film orientations with the major peaks being at ~20 5° in 2-Theta associated with (112)/(200) and ~41° from (224)/(400) facets, which is described to be more beneficial for charge transfer. However, most of the best efficiency perovskite-based solar cells present highly oriented XRD patterns with the same strong intensity peaks than the one observed in this work. This observation usually implies an annealing step and measurements performed at room temperature.[1,30–32]

Very small peaks are also observed in between the two main sets of our $CsPbI_3$ thin films at ~20.2° in 2-Theta attributed

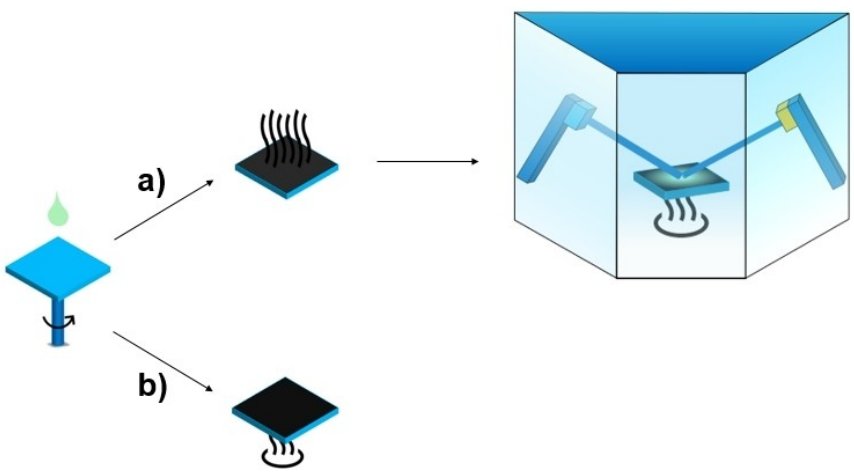

Figure 1. Schematic of spin-coating followed by a) spontaneous evaporation process of thin films and In-situ temperature phase change analysis monitored by XRD technique (Parts 1,2 and 3) and b) flash-annealing thin films fabrication (Part 4).

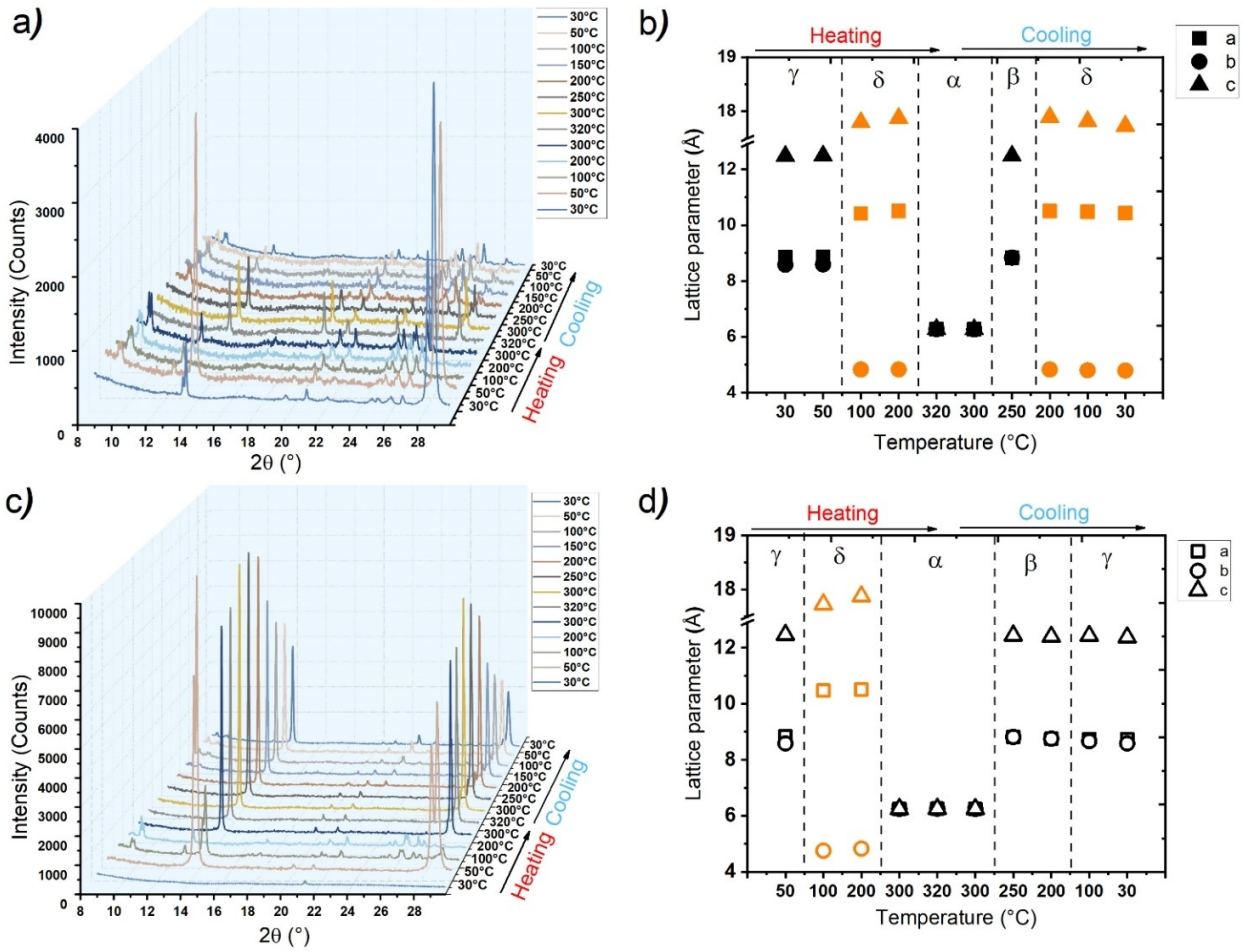

Figure 2. a,c) XRD patterns and b,d) unit cell parameters variations for (top) $CsPbI_3$ and (bottom) mix [$CsPbI_3$ + 2D] thin films upon heating and cooling under nitrogen.

to the (200)/(112) planes, ~22 7° for (210)/(120) planes, ~25° for (202)/(022) planes, or ~27.1° for (212)/(122) planes also characteristic of the gamma phase generally characterized after heat treatment. This black phase remains at 50 °C as shown on the XRD pattern with all main characteristic peaks clearly duplicated. The (hh0) planes are again the most intense lines with a similar intensity for the (002) and (004) planes, as well as for the (110) and (220) planes, which suggests that the film is fully crystalline at this stage. Small intensity peaks characteristic of the delta phase have appeared, showing the relative instability of the black phase of $CsPbI_3$ even though it is kept under blowing nitrogen atmosphere.

The black phase has completely disappeared at 100 °C and the delta phase, corresponding to the yellow orthorhombic phase composed of disconnected octahedra, remains all the way up to 300 °C. The alpha phase appears at 320 °C under nitrogen with sharp peaks at ~14, 20 and 28° in 2-Theta, as described in the literature. The delta phase has completely disappeared and is assumed to be completely converted into the cubic alpha phase. XRD data refinement gives $a = 6.277(1)$ Å unit cell parameter (see Figure 2b), in good agreement with previously reported values.[9,11]

The alpha phase remains pure upon cooling down to 250 °C, with a general peak enlargement suggesting a structural variation consistent with a lower symmetry phase known as the beta phase described elsewhere.[9] At 200 °C, peaks characteristic of the delta phase reappear in majority while those of the black phase disappear, in agreement with Nasstrom *et al.* who showed that thin films of $CsPbI_3$ cooled down in nitrogen showed a phase transformation from the beta to the delta phase at 184 °C.[14] Although previous studies performed on $CsPbI_3$ powders heated up in closed capillary showed that it can then be possible to obtain the gamma phase at RT, thin films are more constrained and can behave differently.[9] The non-perovskite delta phase is here observed all the way down to RT. SEM images of the film after in-situ XRD show particles of less than 1 µm in diameter mostly aggregated and forming smooth areas while pinholes have been formed during the heating process limiting the film compactness, as shown in Figure 4a.

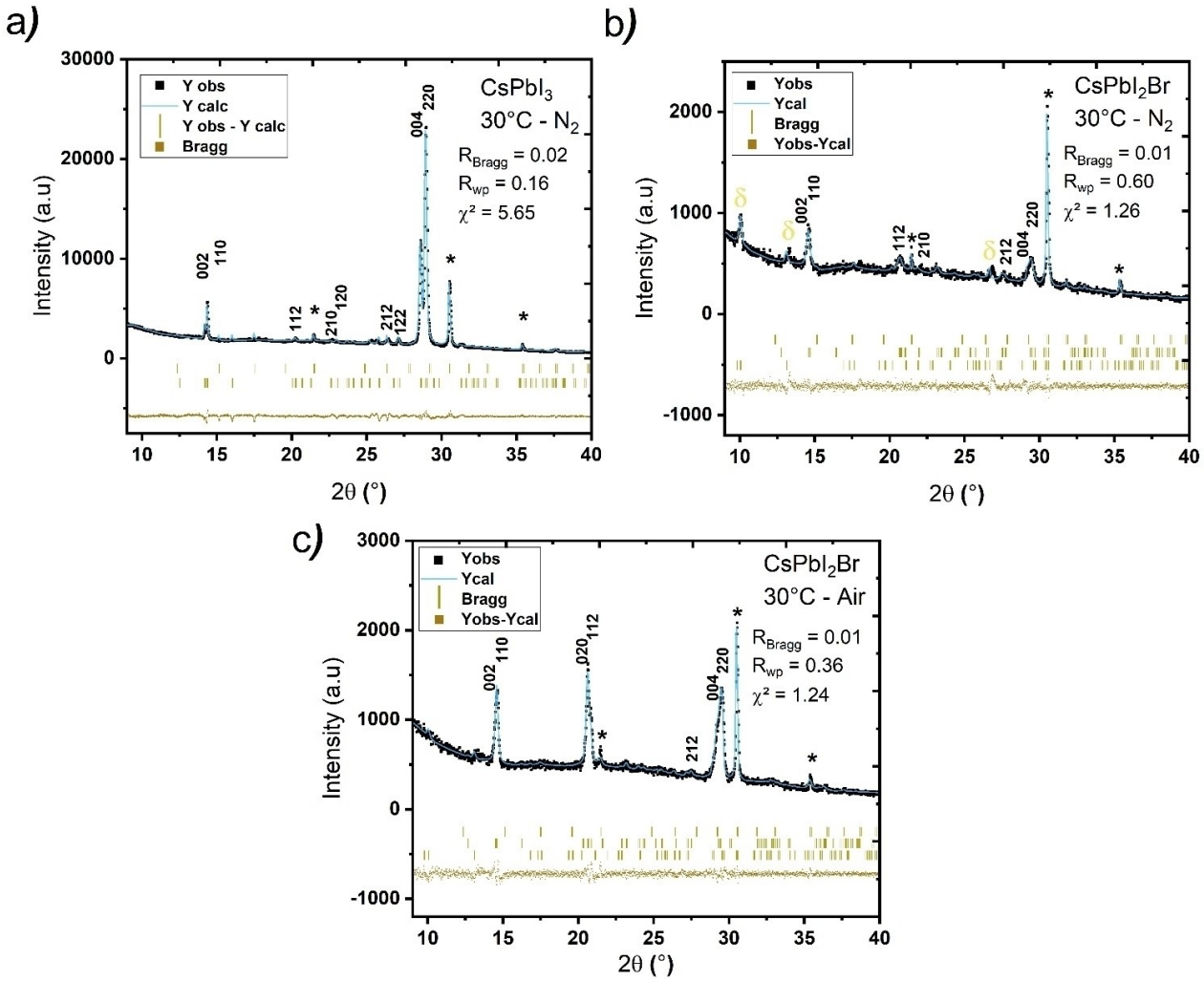

Figure 3. Refined XRD patterns of thin films of a) $CsPbI_3$ in N_2, b) $CsPbI_2Br$ in N_2 and c) $CsPbI_2Br$ in air, using Le Bail's method, with the gamma phase at ambient temperature before heating. * is the ITO substrate.

3D $CsPbI_2Br$ thin films

Bromide is often used to stabilize the all-inorganic $CsPb(I,Br)_3$ family of compounds. With a bandgap of 1.9 eV the black form of $CsPbI_2Br$ is still a very interesting material for photovoltaic applications and a record maximum cell efficiency of 17% was obtained in 2020.[33] $CsPbI_2Br$ thin films were prepared as described above, from salt precursors in solution with DMSO, spin-coated in air at RT and quickly introduced in the XRD chamber for in-situ analysis under nitrogen atmosphere.

In-situ XRD patterns and refined lattice parameters are shown in Figure 5a and Figure 5b. Based on the XRD peaks observed, we can say that thin films of $CsPbI_2Br$ spontaneously crystallize at 30 °C to form a black phase, similarly to $CsPbI_3$, without any trace of the delta phase. Main peaks at ~14.6°, 20.6°, 29.2° in 2-Theta, characteristics of the black phase, contain two contributions each that can be indexed with the gamma structure. Unit cell parameters obtained after pattern matching are $a = 8.602(5)$, $b = 8.454(6)$ and $c = 12.146(2)$ Å, consistent with a smaller cell volume in comparison to the unit cell of the gamma phase of $CsPbI_3$ determined at the same temperature, due to the smaller size of bromide compared to iodide on the *X* site of the distorted ABX_3 perovskite. Peaks are broader here than for $CsPbI_3$, suggesting smaller crystallite size and/or constraints, and there is no preferred orientation. Although the delta phase appears at 50 °C and becomes more and more important as the temperature increases, the black phase remains upon heating. We performed profile refinement at each temperature and observed a tendency for homogenization of the cell parameters with *a* and *b* merging at 200 °C, that could also be refined with the beta phase usually observed upon cooling (see Figure S2b). At 300 °C, XRD peaks become sharper and the cell can be refined in the cubic symmetry with $a = 6.154(1)$ Å (see Figure 5b and Figure S2e). The unit cell parameter is equal to 6.158(1) Å at 320 °C. The fact that it is cubic at a lower temperature than for $CsPbI_3$ is also consistent with the bromine influence over the transition temperature. Our cubic lattice parameter determined at 300 °C is close to the

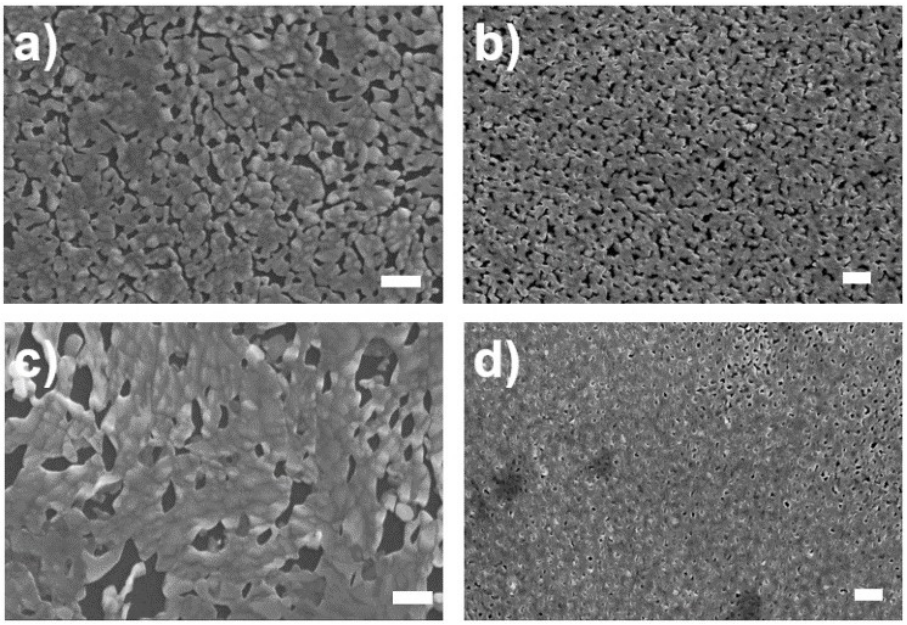

Figure 4. SEM images of a) $CsPbI_3$, b) $CsPbI_2Br$, c) mix [$CsPbI_3$ + 2D] and d) mix [$CsPbI_2Br$ + 2D] thin films after in-situ XRD analysis under nitrogen (scale bar = 4 μm).

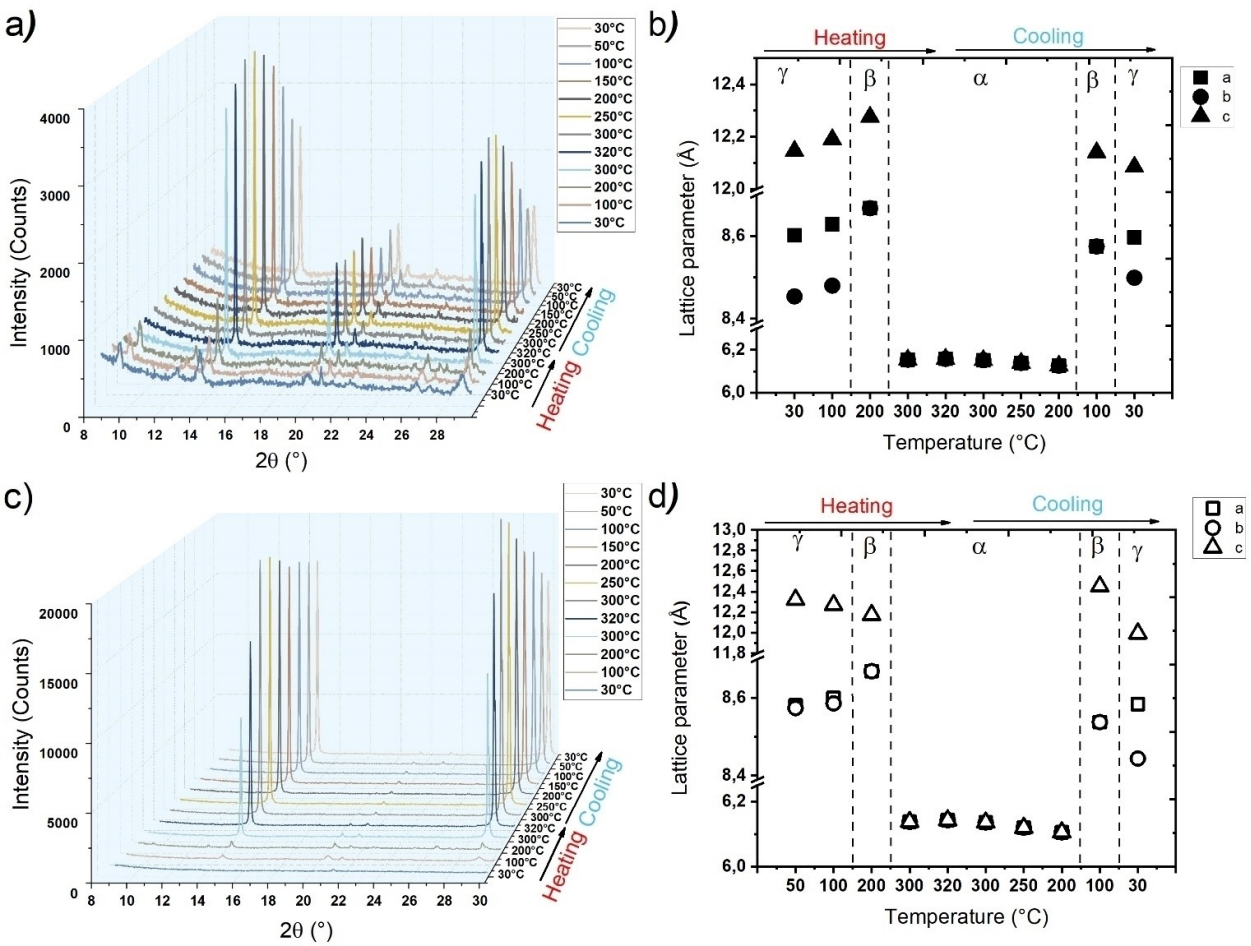

Figure 5. a,c) XRD patterns and b,d) unit cell parameters variations for (top) $CsPbI_2Br$ and (bottom) mix [$CsPbI_2Br$ + 2D] thin films upon heating and cooling under nitrogen.

value reported in the literature for $CsPb(I_{1-x}Br_x)_3$ with $x \sim 1/3$, that was $a = 6.170$ Å, where no black phase was characterized upon heating for $x < 0.5$, even after pre-heat treatment of thin layers.[14] Yet, EDX analysis performed on our $CsPbI_2Br$ thin films, which showed 45(2) mol.% of I and 21(2) mol.% of Br, confirmed the close $CsPbI_2Br$ stoichiometry (experimentally $CsPbI_{2.05}Br_{0.95}$ (see Figure S3b).

Upon cooling thin films in nitrogen flow, XRD data analysis show that only the black phase of $CsPbI_2Br$ is observed all the way down to RT, in opposition to $CsPbI_3$ for which the delta phase was leading preponderant below 200 °C upon cooling. XRD peaks enlargement suggest a loss of the cubic symmetry and small octahedral distortion. At 100 °C, a tetragonal-like structure (with *P4/mbm* space group) can be refined with $a = b = 8.575(1)$, *and* $c = 12.140(1)$ Å. At 30 °C, XRD peaks exhibit shoulders and the phase can be refined with the gamma phase with $a = 8.597(1)$, $b = 8.499(1)$ and $c = 12.085(5)$ Å unit cell parameters, which is less distorted than the starting black gamma phase before heating where the unit cell parameters were $a = 8.602(5)$, $b = 8.454(6)$ *and* $c = 12.146(2)$ Å. Large grains of a few micrometers and good thin film compactness were observed by SEM analysis after in-situ measurements (See Figure 4b). Better film compactness in comparison to $CsPbI_3$ might be attributed to the conservation of the orthorhombic gamma phase instead of the strongly distorted delta orthorhombic delta phase, though holes are observed in both cases.

Therefore, $CsPbI_2Br$ thin films can be prepared with the black phase at room temperature, just like $CsPbI_3$, but its higher stability can allow us to observe phase transitions upon heating that are close to the ones observed upon cooling. Bromine substitution is clearly verified to improve perovskite phase stability in this case, avoiding the transition to the delta phase.

In-situ XRD analysis of 3D inorganic halide perovskites in the presence of 2D $Cs_2PbCl_2I_2$ under nitrogen atmosphere

A route to stabilize halide perovskites is to form separate perovskite blocks or lower dimensionality materials which can significantly influence stability, electronic structure and physical properties. The integration of the recently discovered 2D Ruddlesden-Popper's structural type $Cs_2PbCl_2I_2$ was used in order to increase the phase stability and study its influence over the thermal behavior of the phases as well as thin films orientation and morphology. 2D $Cs_2PbCl_2I_2$ material can be synthesized in a liquid solution by using the appropriate amount of CsI and $PbCl_2$ salt precursors with DMSO (see Figure S4). We prepared a mixture of a so-called 3D perovskite ($CsPbI_3$ or $CsPbI_2Br$) with 2D phase in DMSO and performed in-situ XRD analysis on freshly spin-coated films. It is noteworthy that the presence of the small quantity of 2D phase in the mixture could only been evidenced in the first stages of our experimental work while optimizing the film quality, when preferred orientation of the 3D major phase was not too strong and/or after film degradation in air (See Figure S5 and Figure S6).

Mix [3D $CsPbI_3$ + 2D] thin films

XRD data of a stoichiometric mixture of halide precursors spin-coated as a thin layer at RT in order to obtain the 3D $CsPbI_3$ phase and 7.5 mol.% of 2D $Cs_2PbCl_2I_2$ together after evaporation of DMSO are shown in Figure 2c. Only the XRD lines corresponding to the ITO substrate can be observed at 30 °C in nitrogen, suggesting that the presence of the 2D phase slows down the crystallization process of the mix [3D + 2D], in comparison to the data described above. At 50 °C, a pure crystalline orthorhombic perovskite phase can be indexed corresponding to the gamma phase of $CsPbI_3$ (See Figure S7). The unit cell parameters are $a = 8.838(5)$, $b = 8.584(4)$ *and* $c = 12.464(1)$ Å, which correspond to a small cell contraction in comparison to pure $CsPbI_3$ gamma phase. This effect might be due to the 2D-anchored effect during crystallization and growth or to the partial substitution of iodine by chloride.[23,34–38] The two main sets of peaks observed at ~14.4 and 28.9° in 2-Theta suggest a strong preferred orientation along the [00 l] and [hh0] directions even more favorable here in the presence of the 2D phase in comparison to the observations made without it. Also, the lower intensity value of the second peak at ~28.9° in 2-Theta compared to the one at 14.4° might be due to the slow phase transformation of the black phase toward the yellow phase during the XRD scan. Thus, if the black phase appears spontaneously in all-inorganic cesium lead halide perovskites it is still highly unstable for high iodine content, even with 2D phase addition. At 100 °C, the relative intensities of the gamma phase have strongly decreased compared to those observed before at 50 °C and the XRD peaks characteristic of the delta phase are now present at 9.9°, 13° and 26°, for instance. This delta phase is then the main phase observed until 200 °C.

The alpha phase is fully formed at 300 °C (with $a = 6.250(1)$ Å), which is 20 °C before the temperature measured for the single $CsPbI_3$ phase in the same conditions. At 320 °C the pure cubic phase remains, with $a = 6.255(1)$ Å. The peak at ~20° in 2-Theta, attributed to the (110) line in the cubic form, is hardly seen whereas the intensities of the peaks measured at 14.2 and 28.5°, corresponding respectively to the (100) and (200) planes, are very strong, suggesting a preferred orientation along the crystallite cubic faces. Upon cooling, the mix [3D + 2D] undergoes structural changes. At 250 °C, XRD peaks start to split due to a loss in degree of symmetry and a structural transformation. A tetragonal-like structure was used to refine the phase obtained at that same temperature and the profile fitting shows good reliability factors with the *P4/mbm* space group *and* $a = b = 8.816(1)$ *and* $c = 12.441(1)$ Å cell parameters. A more significant distortion is observed at 100 °C and the gamma phase is the major phase down to room temperature, with $a = 8.736(1)$, $b = 8.665(1)$ *and* $c = 12.430$ (1) Å, with other small peaks characteristic of the delta phase that are visible in the XRD data. Therefore, the black form of $CsPbI_3$ thin films can be kept down to RT in the presence of the 2D phase, though it is not perfectly pure.

The comparison between the XRD data of $CsPbI_3$ and mix [$CsPbI_3$ + 2D] in nitrogen shows that crystallization is slowed down by the 2D additive, starting at 50 °C instead of 30 °C for

the former compound alone. The gamma phase disappears at 100 °C for pure $CsPbI_3$ while it remains for the mixture of $CsPbI_3$ and 2D phase at this temperature. The delta phase takes over upon further heating even though working in nitrogen and the alpha phase appears ~20 °C earlier in the presence of the 2D additive. As the temperature is decreased, the delta phase reappears at 200 °C for $CsPbI_3$ while the black phase is largely dominant all the way down to RT when the 2D phase is present. Small peak enlargements and splits are observed upon cooling which are typical of the black cubic-to-tetragonal-to-orthorhombic phase transformations. The gamma phase is kept for at least 10 hours under nitrogen conditions, and only for a few minutes once exposed to the air. As all-inorganic perovskites are known to be thermodynamically unstable and very sensitive to moisture, here we expect that 3D/2D growth favors the conservation of the black phase. After in-situ XRD analysis, the film was observed by SEM (Figure 4c). Grains of a micrometer scale are visible with strong aggregation and elongation in some places and larger pinholes than for the single $CsPbI_3$ phase treated in similar conditions.

Mix [3D $CsPbI_2Br$ + 2D] thin films

The effect of the 2D phase over the growth and stability of the 3D $CsPbI_2Br$ thin films was also investigated by in-situ XRD in nitrogen. Figure 5c and Figure 5d show respectively the XRD data and the unit cell parameters variations as a function of temperature.

At 30 °C, only the ITO substrate peaks were defined, showing that the presence of the 2D phase slows down the process of crystallization, similarly to the mix [$CsPbI_3$ + 2D]. At 50 and 100 °C, XRD peaks characteristic of the gamma phase are present but intensities are low, suggesting a poor crystallinity in the material and/or small particles at those temperatures. At 200 °C, extra peaks due to the delta phase are present but the black phase transformation can be analyzed. Unit cell parameters correspond to a tetragonal phase ($a = b = 8.669$ *and* $c = 12.175$ Å) and a transition from black orthorhombic to tetragonal symmetry can be identified close to this temperature (see Figure 5d). Upon heating to 300 °C, sharp peaks corresponding to a single alpha cubic structure are obtained and the XRD data refinements give $a = 6.138(1)$ *Å* ($a = 6.143(1)$ *Å* at 320 °C). A strong phase orientation is evidenced, once again as observed for the mix [$CsPbI_3$ + 2D].

No phase change was observed upon cooling down to 200 °C. The cubic cell volume decreased. As temperature reached 100 °C, peak enlargements suggested a change to a lower symmetry than for the cubic phase. Our refinements using the Le Bail method showed that tetragonal phase reappeared at least at 100 °C with for instance the peak at ~23° in 2-Theta corresponding to the (210) planes. Gamma phase is characterized at 30 °C with $a = 8.584(1)$, $b = 8.444(1)$ *and* $c = 11.995(1)$ Å cell parameters. Peak shapes are narrow at ambient temperature suggesting only a small octahedral distortion and the black phase is still highly oriented. Interestingly, when comparing the XRD data from the highest temperature down to RT with and without the 2D phase, we can thus notice that the presence of the latter phase favored a preferred orientation along the [00 l] direction, for both $CsPbI_3$ and $CsPbI_2Br$. Indeed, the peak intensity of the (110) planes around 20° in 2-Theta of the high temperature alpha phase is largely observed upon cooling for the single 3D phases, while it becomes hardly visible in the presence of a small quantity of the 2D phase, suggesting then a preferential orientation or film texture that is kept down to room temperature and might contribute to the black phase stabilization. Films heat-treated in these conditions analyzed by SEM are compact with a rough surface, a few pinholes, and some elongated particles probably due to the 2D phase (see Figure 4d).

Preferential orientation effect originating from 2D $Cs_2PbI_2Cl_2$ addition has been shown by Li et al. in a recently published paper, where thin film orientation and 2D anchored 3D phase allowed to stabilize $CsPbI_{2.5}Br_{0.5}$ black phase with a better film density.[23] An improved power-conversion efficiency (from 6.6 to 14.4%) was measured in a photovoltaic device, which was attributed to a better film compactness, increased defect passivation, bigger grain size, and preferred orientation. The film quality is assumed to reduce the thermodynamic barriers generally observed at grain boundaries, as well as trap states acting as recombination sites. In our case, the presence of the secondary 2D phase slows down and restrains or forces the 3D phase crystal growth to a preferred crystal orientation on the flat substrate that would facilitate the preservation of the black phase in thin films.[13]

The stabilization mechanism of the mix [3D + 2D] was described by using TEM images.[23] Although we propose that the phase stabilized at room temperature is rather orthorhombic than cubic, it is likely that the lattice mismatch between the 2 phases is very low and that distortion can occur at the interface. Calculations of Pb Pb bond lengths show a lattice mismatch comprised between 8.7% and 9.8% (calculated for two different Pb Pb distances in the orthorhombic structure of 6.18 and 6.25 Å, and for the 2D structure with 5.64 Å) for the 3D/2D (110)/(003) interface. As observed in a recent work, it is possible for a soft perovskite lattice to induce strain relaxation mechanism at the interface of a film by octahedra tilting to form a coherent interface.[39] This tilt happens because of a symmetry or small lattice parameter mismatch. Kepenekian et al. showed that layered hybrid perovskites exhibit a mechanical energy relaxation more efficiently than for 3D perovskites, which is attributed to the additional freedom degree induced by the vacant space in between the octahedra plans.[40] Thus, it is possible that a coherent interface is created between the 3D and 2D phases during the co-crystallization stage, even more favored as the chemical composition of both phases is very close ($CsPbI_xBr_y$ and $CsPb_{0.5}I_{1.5}Cl_{1.5}$ expressed for a mole of cesium).

In-situ XRD analysis of 3D $CsPbI_2Br$ and mix [3D $CsPbI_2Br$ + 2D] thin films in air

3D $CsPbI_2Br$ thin films

Since $CsPbI_2Br$ appears more stable than $CsPbI_3$, we chose to analyze the first compound prepared as a freshly spin-coated thin film by in-situ XRD, in air. Therefore, all the process described in the following (from the liquid solution preparation, spin-coating to the thin layer analysis in the XRD chamber) was performed in normal conditions. XRD patterns variations are shown in Figure 6a. As observed for $CsPbI_2Br$ under nitrogen, the film spontaneously crystallizes at 30 °C. The peak observed at 20.6° in 2-theta here appears with a higher intensity than those at 14.6 and 29.4°, suggesting a less oriented and textured film in air compared to the layers prepared in blowing nitrogen. All sets of peaks are wide, suggesting a peak split, and can be refined with an orthorhombic symmetry characteristic of the gamma phase. Cell parameters are then $a = 8.743(2)$, $b = 8.527(1)$ *and* $c = 12.140(1)$ Å at 30 °C. No delta phase was observed at this temperature, but the non-perovskite material appeared at 50 °C and remained as a secondary phase until 200 °C. Although kept in a closed chamber during the XRD measurements, the sample was loaded in air containing moisture with ~40% relative humidity (RH) at 20 °C, which is detrimental to perovskite stability. Unit cell parameters of the black phase were determined by using the Le Bail method. They all increase with temperature and a tetragonal phase can be characterized at 200 °C with $a = b = 8.664(1)$ *and* $c = 12.266(1)$ Å (see Figure S2c). At this temperature, it is likely that thermal energy is not sufficient to activate octahedra oscillations assimilated to cubic structure, but progressively make *a* and *b* lattice parameters match each other. Upon further heating, the black phase peaks get very sharp at 250 °C and can easily be indexed with the alpha phase, with $a = 6.145(2)$ Å, while no other phase is observed. As mentioned in the literature, the cubic phase probably corresponds to a randomly distributed and oscillating $[PbI_6]^4$ octahedra which is averaged and identified as – but not exactly – cubic.[11] If heated at a temperature above 300 °C in air, films are destroyed as XRD peaks are quickly lost, certainly due to halide vaporization and material decomposition/oxidation in these conditions.

Upon cooling, two structural transitions can also be characterized in air, with the beta phase observed at 150 °C and

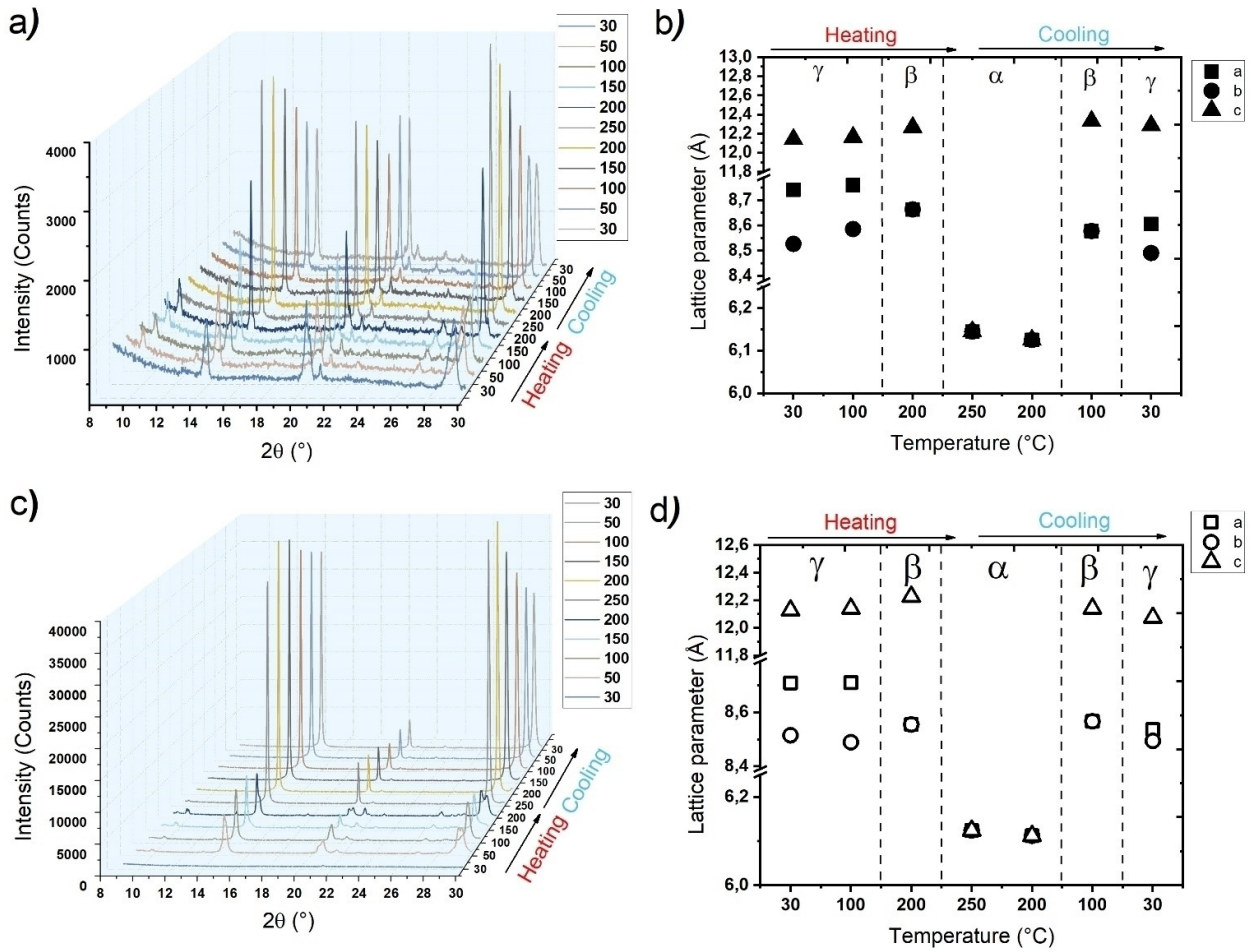

Figure 6. a,c) XRD patterns and b,d) unit cell parameters variations for (top) $CsPbI_2Br$ and (bottom) mix [$CsPbI_2Br$ + 2D] thin films upon heating and cooling in air.

the gamma phase at 30 °C. A single gamma phase is there obtained at room temperature in air and remains as such overnight. Once the sample was removed from the XRD chamber, a film color change was observed within a few minutes, as shown in Figure 7. We expect that the relative humidity is reduced in the XRD chamber during the in-situ temperature cycle, and that there is no air flux that contributes to destabilize thin films. Thus, the black perovskite is stable for a far longer time under dry air and closed systems than in open space and under 40% RH. The three main peaks that we focused on during our XRD analysis are similar in intensity, evidencing for no particular orientation of the film while heated and cooled down in air atmosphere.

Mix [3D $CsPbI_2Br$ + 2D] thin films

In-situ XRD patterns of the mix [$CsPbI_2Br$ + 2D] as a function of temperature are shown in Figure 6c. The first scan performed at 30 °C after ~15 min in the XRD chamber did not show any XRD peak apart from those of the ITO substrate, similarly to the same 3D/2D mixture introduced in nitrogen. At 50 °C, the gamma phase can be identified and refined parameters are a = 8.710(1), b = 8.515(1) and c = 12.127(1) Å (see Figure 6d), with no preferred orientation noticed, while the film obtained before, for the same composition in nitrogen, was textured and showed different unit cell parameters (with a = 8 581, b = 8.574 and c = 12.323 Å). We assume that air moisture must have a strong impact over the crystal growth after spin-coating. The 2D phase used in dry atmosphere will favor thin film orientation. The solvent used in our work (DMSO) is known to be very hygroscopic and has a high boiling temperature. Thus, it is likely that during the in-situ scan under air, moisture is quickly adsorbed and absorbed in the film and can deeply modify the crystal growth process. A tetragonal phase was successfully used to refine the XRD scan measured at 200 °C with a = b = 8.555(1) and c = 12.227(1) Å. At 250 °C, the cubic structure is formed (with a = 6.124(1) Å) and stronger intensities for the peaks at 14.5 and 29 2° in 2-Theta evidencing for a preferential orientation here in the presence of the 2D phase.

Upon cooling, an extra main peak observed at 23.2° in 2-Theta at ~100 °C, attributed to the (210) planes, suggests a tetragonal phase that can be fully indexed and refined. Gamma phase can be refined from 50 °C down to room temperature with a preserved preferred orientation of the crystals. Even though the peak intensity at 20.2° in 2-Theta is here higher than for the same sample measured in nitrogen atmosphere, a texturing trend is also observed in air. 2D-induced preferential growth seems to be independent of the atmosphere conditions. The texture of pure $CsPbI_2Br$ is different and also depending on the environmental atmosphere. Moisture level can influence the growth of perovskite polycrystalline film from a liquid solution.[41] Li and coworkers showed that such 3D/2D solar cell kept 80% PCE during 16 hours under high moisture condition, when controlled sample of 3D phase lost more than 50% efficiency within a few hours.[23] Therefore, the 2D structure of $Cs_2PbCl_2I_2$ seems to favor the preferred orientation growth of the main 3D-type structure and limits moisture penetration inside the mix [3D + 2D], which is beneficial for thin film texturing during crystallization, and improves carrier mobility as well as stability even under moisture loaded ambient air. Our main results related to the in-situ XRD data analysis are schematized in Figure 8. The black orthorhombic phase of 3D $CsPbX_3$ (with X=I, Br) is formed spontaneously at ambient temperature. It undergoes two transitions upon heating, to a tetragonal and cubic phases, respectively. The reverse transitions are observed upon cooling down. The black phase is stabilized in the presence of a 2D phase.

Some recent studies showed that pressure, temperature, epitaxial growth or additive phase can have a strong influence on the system formation and stability of 3D halide perovskite films.[13,30,42] The peak shape analysis can sometimes give valuable information about the crystallite size and micro-strains, using the Williamson-Hall method, for instance. Indeed, strain engineering operated in several works showed that there is a tendency to improve the stability while reducing strain, or more precisely applying compressive strain to perovskite films.[13,22,30,42–45] Such parameter analysis could actually shed a light on the differences observed on perovskite materials in the powder and thin film states. A compressive effect on the Pb I bond is expected to improve electronic orbitals overlap and to reduce significantly the bandgap of FAPI from 1.55 to 1.44 eV for 1% tensile strain and 1% compressive strain, respectively. Moreover, the thermodynamic barrier and activation energy are significantly influenced by strains, as compressive strain has been calculated to increase activation energy for black to yellow phase transition, thus improving perovskite phase stability. A study on $CsPbI_3$ powder also confirmed results observed on this films, showing that applying pressure in ambient conditions allows the gamma phase preservation even

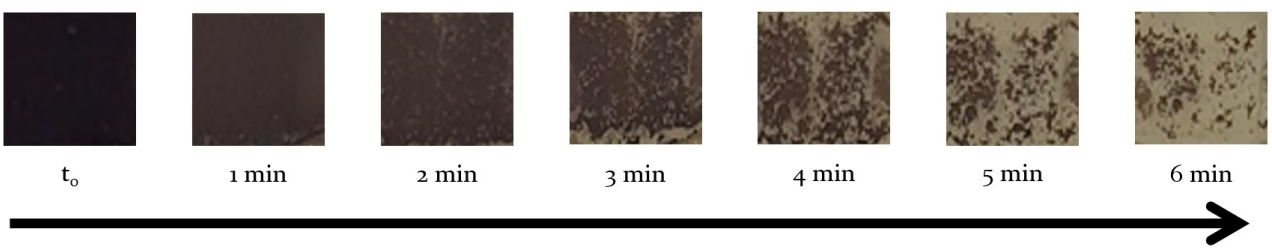

Figure 7. Photography of $CsPbI_2Br$ thin films after in-situ XRD analysis in air once removed from the XRD chamber and exposed to ambient conditions.

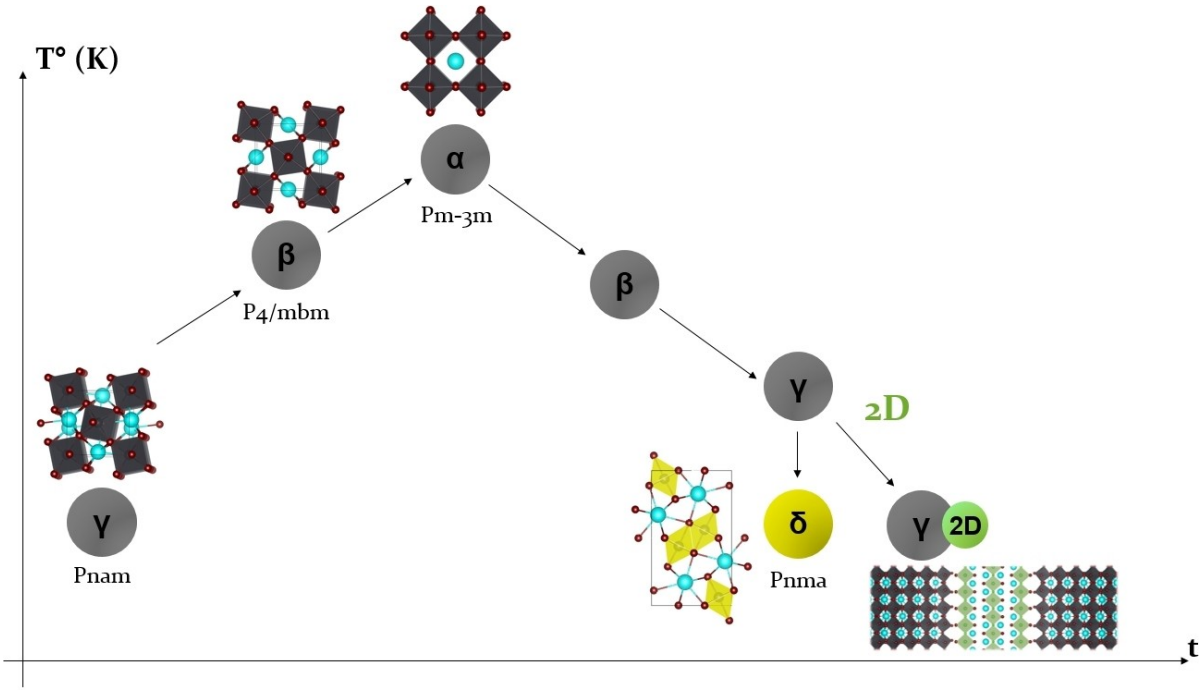

Figure 8. Schematic representation of the all-inorganic structural variations determined on thin films by in-situ XRD analysis (based on Marronnier et al. [9]).

in moisture loaded air.[46] This improved stability was further explained by DFT calculations indicating a tilt in $[PbI_6]^4$ octahedra which favors the gamma phase instead of the delta phase.[47] In this work, XRD peak widths were usually too small to be able to strictly use Williamson-Hall method. However, these in-situ XRD results obtained in air were used for thermal expansion coefficient determination for both 3D and [3D + 2D] phases. Strains were then calculated on flash-annealed thin films in the following part.

3D $CsPbI_2Br$ and mix [$CsPbI_2Br$ + 2D] thin films flash-annealed in air

In-situ XRD measurement performed on freshly spin-coated films was proven to be very fruitful for crystalline phase determination and transformation. But it does not provide an ideal set up for the preparation of compact and smooth thin films. Usually, quality thin films necessitate a quick heating step at a moderate temperature.[6,30] Thus, we performed phase identification by XRD at various heating stages just after spin-coating to observe the influence of the 2D phase addition on the deposited film in these circumstances (Figure 1b). Thin films preparation was realized in air with a relative humidity level close to 40 %. Samples were annealed at each temperature until the black phase was visually covering the full substrate and left for the same amount of time on the heating plate in order to obtain a fully crystalline material before removal (see Table S1). This preparation procedure was based on a previous study, and allows to obtain fully crystallized thin films while minimizing the delta phase formation.[48]

All XRD patterns recorded at the same temperatures than for the first parts of this paper are plotted in Figure 9. For the samples heated at low temperature, split peaks are clearly visible, that would correspond to the gamma phase. As we heat quickly the sample at a higher temperature thin films are crystallized in a less distorted structure that remains upon fast cooling. Indeed, XRD data show a peak sharpening for the highest temperatures and that cell parameters are closer than for the lowest temperatures (see Figure 9). Normalized parameters to the pseudo-cubic cell (a and b divided by $\sqrt{2}$ and c divided by 2) show that all cell parameters are getting closer when temperature annealing is higher than 200 °C, for both 3D and mix [3D + 2D] phases (see Figure S8). A previous study showed that it is possible to thermodynamically stabilize the beta phase of $CsPbI_3$ by applying a passivating surface treatment.[1] This observation suggests the formation of a distorted orthorhombic structure induced by the flash annealing treatment. We can also notice that all three main sets of peaks at ~14.6, 20.2 and 29° have similar intensities for the single 3D phase while those at 14 and 28° are stronger when the 2D phase has been added. This observation tends to confirm our previous report about the preferential orientation of the films with the (002) and (110) planes in the presence of the 2D phase, in a humid environment that is more evident in this case than in the close XRD chamber.

SEM images of thin films of $CsPbI_2Br$ as a single phase and mixed with the all-inorganic 2D phase are shown in Figure 10 for different flash-annealing temperatures. Thin films show poor substrate coverage from 30 °C to 100 °C, either with or without 2D phase. Since DMSO boiling temperature is ~190 °C, we suppose that the solvent evaporation might contribute to the

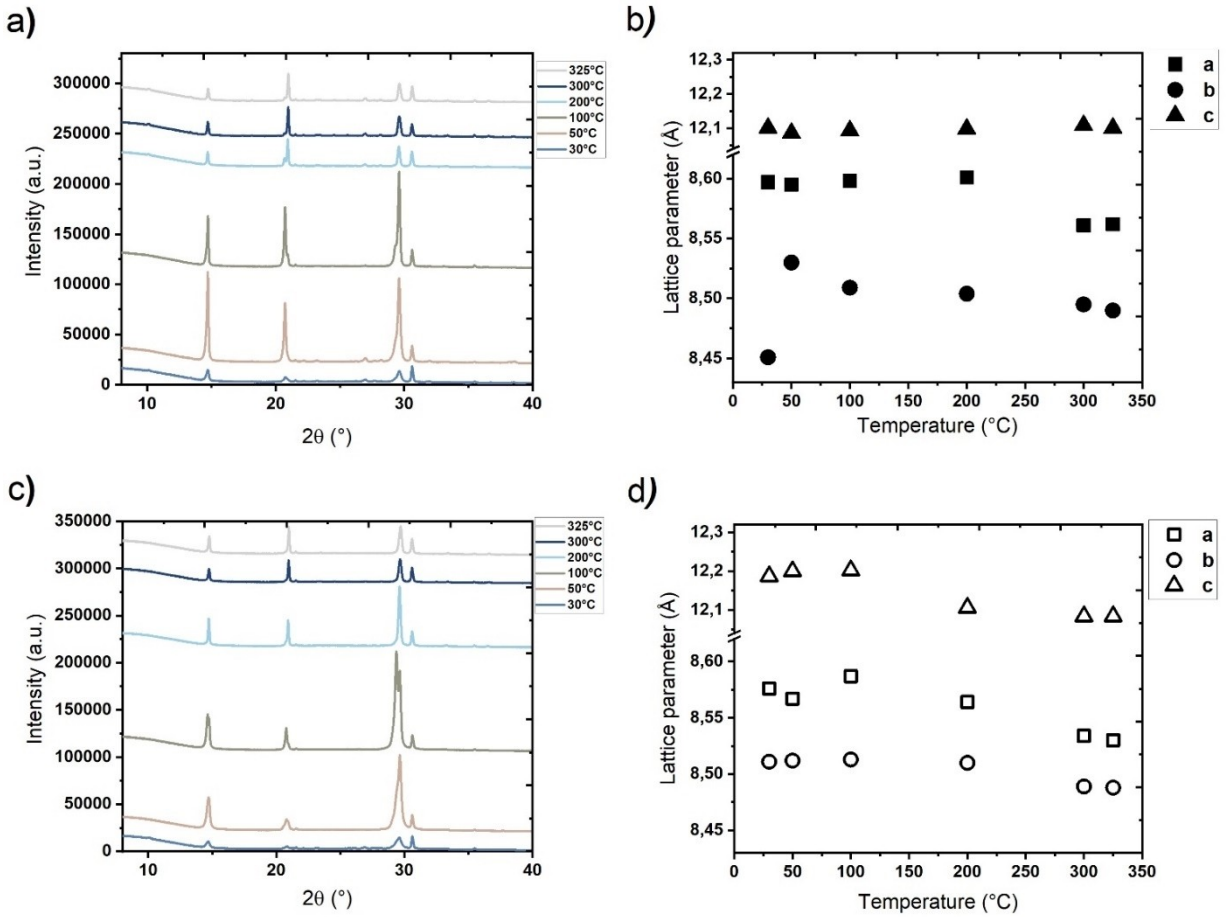

Figure 9. a,c) XRD patterns and b,d) unit cell parameters variations for (top) 3D $CsPbI_2Br$ and (bottom) mix [$CsPbI_2Br + 2D$] as a function of the flash-annealing temperature in air.

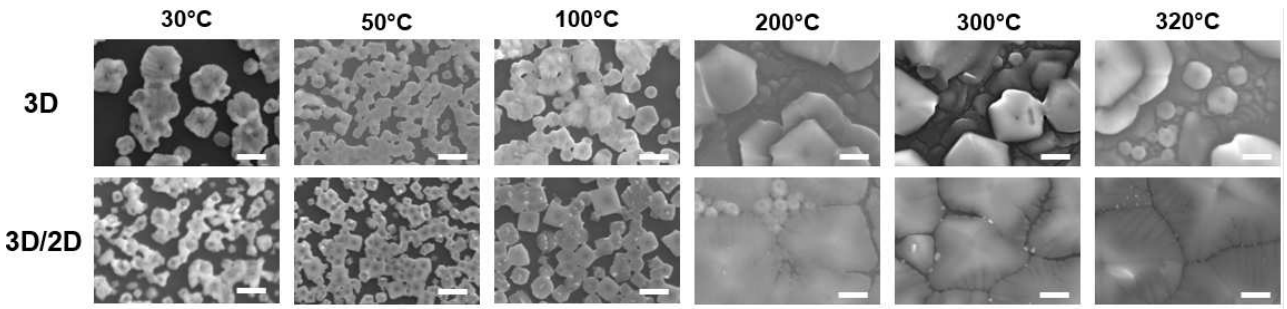

Figure 10. SEM images of (top) 3D $CsPbI_2Br$ and (bottom) mix [$CsPbI_2Br + 2D$] flash-annealed thin films at different temperatures (scale bar is 2 μm).

formation of the big isolated crystals there observed at low temperature. The water penetration might also contribute already to the fast film degradation. Grain size is lower than 2 μm in diameter and grain shapes are different from the 3D phase to the mix [3D + 2D] layer, varying from a round shape to a square-like particle that can be related to the preferential orientation observed by in-situ XRD analysis.

When films are heated at higher temperatures (200, 300 or 325 °C), grain size is generally over 5 μm in average and increasing with a temperature, which is consistent with previous work on the same composition.[49] For 3D samples, big overlapping plates are separated by smaller particles just like water lilies, exhibiting crevices and holes. This inhomogeneity would be detrimental to a solar cell, enhancing short-circuit and charge carrier recombination. Different morphologies are observed in the presence of the 2D phase. Grains are tight with each other and their size is logically increased with the temperature. Grain boundaries are small and the films are more

compact than for the 3D phase alone. Although it was not possible to clearly distinguish the 2D from the 3D phase by SEM analysis, it is likely that tiny particles of needle shape close to the grain boundaries might be related to the 2D phase inserted in between the major 3D grains. XRD data analysis confirm that the presence of the 2D phase stabilizes the black phase, at 200 and 300 °C (see Figure S9 and Figure S10). Thin films of the mix [3D + 2D] material flash-annealed at 300 °C remained black for the longest time (~ 100 hours) in ambient conditions (20 °C, 50 % RH) (see Figures S9, S10 and S11). This observation is confirmed by XRD analysis patterns that show the preservation of black phase for a longer time for mix [3D + 2D] material.

To better understand the increased stabilization of perovskite thin films with increasing annealing temperature and in the presence of the 2D phase, we used the in-situ XRD measurements performed in air (Part 3) to plot the variation of the inter-reticular distance (corresponding to the 2-Theta = 14.6° diffraction peak) as a function of temperature in Figure 11. As expected, we observe a small shift of the diffraction peak towards lower values corresponding to an increase in d-spacing upon heating. This corresponds to a lattice expansion that is proportional to the increasing temperature in the XRD chamber. By plotting the deformation ε *vs* T, one can determine the thermal expansion coefficient α from the slope of the graph, as described in the literature for the same type of perovskite structure (see Figure S12).[45,50] The coefficient calculated for the 3D phase is higher (larger slope value) for the 3D material alone than for the mix [3D + 2D] film with $\alpha = 3.3$ and $2.2*10^{-5}\ K^{-1}$ respectively. The values obtained are also very close to the one reported in the literature for the $CsPbI_2Br$ phase, where values range from 3.3 to $8.4*10^{-5}\ K^{-1}$.[45,51]

The expansion of the 3D phase seems minimized by the integration of the 2D phase in the thin film. Strain is defined as the deformation of a solid due to stress. The plot of the evolution of the strain parameter ε as a function of the flash-annealing temperature shows that when temperature is increased, a cell shrinkage is observed, as ε tends to negative values. This corresponds to a lattice compression in the direction perpendicular to the substrate. The stress in thin films is already well described in the literature with the grain boundary model pointing that in-plane tensile strain is a consequence of grain boundaries in such material morphology.[52] If we compare the data here obtained, we observe that the lattice contraction is approximately 4 times higher for the mix [3D + 2D] thin film than for the single 3D phase. Since the thermal expansion coefficient of the mix phase is lower, we expect that it does not expand much upon flash-annealing but 2D phase allows to gather strains that result in compressive stresses upon cooling. Therefore, as observed in many recent studies, it is likely that in this case as well compressive strain explains the improved stability of high temperature annealed mix [3D + 2D] thin layers.[30,42,43,45,53]

Recent studies show that film preparation during the flash-annealing stage processed under nitrogen flux can greatly improve the surface morphology with defect passivation and keep up with 85 % of the initial efficiency (16.6 %) for 100 hours a CsPbI2Br-based film.[54] Also, doping with transition metals such as Fe^{2+} (by using $FeCl_2$) or rare earth like Sr^{2+} or Ba^{2+} can stabilize further this film composition.[54–56] Finally, the film encapsulation in dry atmosphere would further help to preserve the black phase for a longer period of time.

Conclusion

In this paper, we show that $CsPbI_3$ and $CsPbI_2Br$ thin films freshly spin-coated on ITO substrate spontaneously crystallize at 30 °C to form its gamma phase, either in nitrogen or air for the latter composition. The yellow delta phase appears faster in $CsPbI_3$ than for $CsPbI_2Br$, especially upon heating. The black

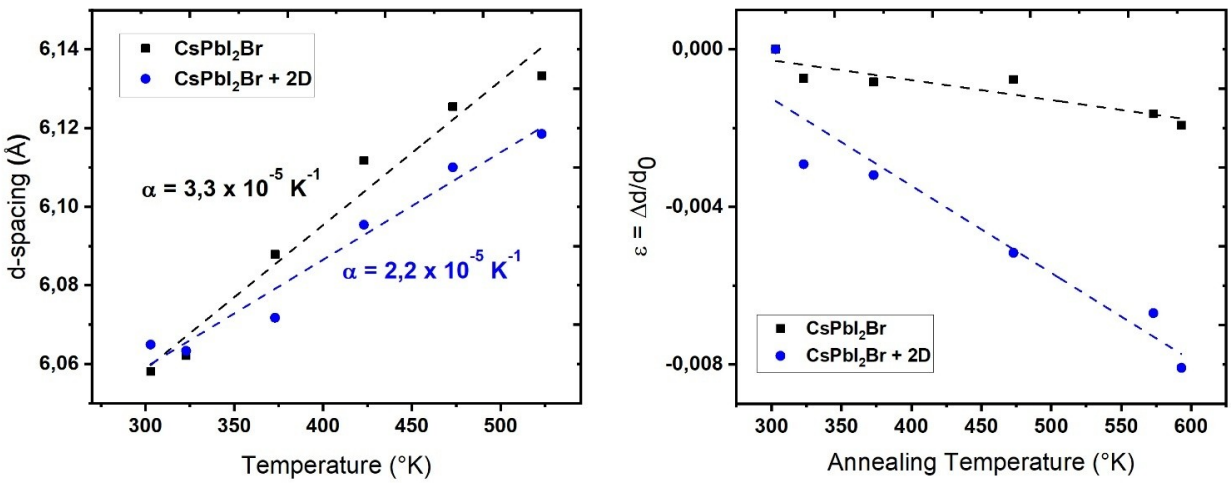

Figure 11. a) Inter-reticular distance variation upon heating in air during in-situ XRD measurements and b) strain parameter variation as a function of the annealing temperature for $CsPbI_2Br$ (black square close symbols) and mix [$CsPbI_2Br$ + 2D] (blue circle open symbols).

phase remains for $CsPbI_2Br$ up to 320 °C in nitrogen or 250 °C in air. Phase transitions from orthorhombic to tetragonal to cubic structures were characterized upon heating for the black phase and reversibly upon cooling. The addition of 2D Ruddlesden Popper's structure type $Cs_2PbCl_2I_2$ improves the black phase stability. The 2D phase enhances thin film preferred orientations, along the [110] and [002] directions at room temperature, for both $CsPbI_3$ and $CsPbI_2Br$. Finally, the effects of different annealing temperatures for a short period of time (within a few minutes at RT to a few seconds at 320 °C) on the structure and film morphology of spin-coated 3D $CsPbI_2Br$ and mix [3D $CsPbI_2Br$ + 2D] thin films were analyzed at ambient conditions. A less distorted structure is obtained for the highest temperatures and thin films are more compact from 200 °C to 320 °C in the presence of the 2D phase, which helps to keep the black phase for a longer period of time.

Experimental Section

Materials and solution preparation

Cesium iodide (99.9% grade CsI), Lead iodide (99% grade PbI_2), were purchased from Sigma Aldrich company. Lead Bromide (98% grade $PbBr_2$) and Cesium chloride (99.5% grade CsCl) were bought from Alfa Aesar and Merck Millipore Corporation, respectively. Dimethyl sulfoxide (99% grade DMSO) and isopropyl alcohol (99.7% grade) solvents were purchased from Sigma Aldrich.

Perovskite precursor solutions were prepared by dissolving 1.4 mmol of CsI and PbI_2 in 1 mL of pure DMSO for $CsPbI_3$ solution. For the mix [3D + 2D] precursor solutions, 7.5 mol.% of 2D phase was used based on the maximized enhanced efficiency and stability showed by Li et al..[23] The corresponding amounts of CsCl and PbI_2 were thus added together to obtain the concentration of 1.4/0.105 molar ratio (3D/2D). Solutions prepared in air were then kept under stirring at room temperature in capped pillbox container for two hours minimum, before being filtered on 0.2 μm polytetrafluoroethylene (PTFE) filter.

Thin films preparation

Substrates used for sample deposition were systematically immerged in acetone, isopropanol, and ethanol under sonication for 15 minutes each. Substrates were then blown with dry air and placed under Ultraviolet-Ozone (UV-O) treatment for 25 minutes using an Ossila UV-Ozone cleaner equipment. Each step was conducted under ambient condition. After UV-O treatment, substrates were immediately used for perovskite film deposition. 50 μL of perovskite solution was deposited with a micropipette on the ITO substrate which was positioned on the SPS Spin 150 spin-coater chuck. The ITO substrate was maintained in position using a vacuum system. Spin-coating of perovskite layer was conducted at 3500 rpm for 30 s and thin films were taken out straight after to perform XRD measurements, or were directly put on a hot-plate for flash-annealing. All our sample preparations were performed in ambient conditions (20 °C – 40%RH) without the use of a glovebox.

Thin films characterization

In-situ experimentations were conducted on a Bruker D8 diffractometer equipped with a Cu X-Ray source in temperature monitoring configuration by using an Anton Paar HTK 1200 N heating system with a heating rate of 0.5 °C/s. XRD scans were performed in the θ-θ Bragg-Brentano geometry directly after spin-coating, since there was good data information on crystallized films. Scans were realized from 9 to 52° in 2-Theta with Cu $K_{\alpha1}$ 0.1541 nm and $K_{\alpha2}$ 0.1543 nm wavelengths and a step scan of 0.016°, straight after annealing to limit moisture induced phase transition. Each scan lasted for 14 minutes. A film thickness of ~300 nm was determined by mechanical profilometry analysis using a VEECO Dektat 3030ST apparatus. Thin films were scratched using a metallic tool, and the step between perovskite layer and the glass substrate was measured with a stylus force of 0,10 mN (10 mg) over 500 μm length. Indium Tin Oxide (ITO) pre-deposited thin film substrates were purchased from Solems Company (ITO SOL 30/1 ~80 nm in thickness obtained by physical vapor deposition on 1.1 mm glass). After spin-coating, thin films (1.5*1.5 cm^2) were quickly transferred (within a couple of minutes) into the XRD chamber and put under nitrogen atmosphere (with a purity of 99.99995% or grade 4.5) when required with a dynamic flux of 1.1 mL/s (4 qnl/h) or left in air in the closed chamber if not otherwise specified. In-situ XRD analysis started at the precise and controlled temperature of 30 °C (reached within 5 minutes max. after insertion in the chamber). Substrates were then slowly heated at a rate of 0.5 °C/s and analyzed up to 250 °C in air or 320 °C in N_2 every 100 °C upon heating and cooling.

XRD data refinements were carried out by using the FullProf package software in pattern matching mode based on Le Bail's method.[57] Full Rietveld refinement is usually more beneficial to precisely determine the structure of a material but harder to perform on thin films, especially if these show preferred orientation along one or a few directions. Indeed, spin-coated processed thin films are generally highly oriented and under strain, making such crystalline structure difficult to refine. Also, a short 2-Theta range was chosen to reduce the chances of a phase transformation during the scan at a particular temperature. Z position and rocking curve were calibrated before thin films characterization. Zero shift, unit cell parameters and peak shape parameters from Caglioti's formula (U, V and W constants) were refined at each temperature. Zero shift was usually negligible (within 0.02° of the initial value) upon heating and cooling. Pattern matching on each XRD data allowed us to justify the crystal symmetry and space group, and to determine the unit cell parameters. ITO peaks were used as an internal standard as its lattice parameters expand far less than for halide perovskites upon heating and are reversible on this temperature range.

For flash-annealed thin layers in air, XRD analysis were realized at RT in air on a BRUKER AXS D4 Endeavor apparatus equipped with a Copper X-ray source and Cu $K_{\alpha1}$ and $K_{\alpha2}$ wavelengths in the θ-2θ Bragg Brentano geometry. Scans were realized from 8 to 60° in 2-Theta with and a step scan of 0.011°, straight after annealing to limit moisture induced phase transition. Each scan lasted for 16 minutes.

Scanning Electron Microscopy (SEM) images were obtained on JEOL JSM6510 LV apparatus equipped with a tungsten source and a secondary emission detector (SE). Energy-Dispersive X-ray Spectroscopy (EDS) was operated on the same apparatus with a Brüker XFlash 6130 system, 1.2 μm spot size and 60 kcps pulse throughput with a 20 kV column voltage at low magnification (x2000).

Acknowledgements

We would like to thank Benjamin Duployer for his precious help for temperature XRD measurements. We also thank FERMAT

federation for giving us the opportunity to operate the analysis on the X-ray Bruker D8 diffractometer.

Conflict of Interest

The authors declare no conflict of interest.

Keywords: $CsPbI_3$ and $CsPbI_2Br$ · $Cs_2PbCl_2I_2$ · Halide perovskites · In-situ X-ray diffraction · Thin films

[1] Y. Wang, M. I. Dar, L. K. Ono, T. Zhang, M. Kan, Y. Li, L. Zhang, X. Wang, Y. Yang, X. Gao, Y. Qi, M. Grätzel, Y. Zhao, *Science* **2019**, *365*, 591–595.

[2] S. M. Yoon, H. Min, J. B. Kim, G. Kim, K. S. Lee, S. I. Seok, *Joule* **2021**, *5*, 183–196.

[3] Y. Meng, M. Ahmadi, X. Wu, T. Xu, L. Xu, Z. Xiong, P. Chen, *Org. Electron.* **2019**, *64*, 47–53.

[4] S. Colella, M. Mazzeo, A. Rizzo, G. Gigli, A. Listorti, *J. Phys. Chem. Lett.* **2016**, *7*, 4322–4334.

[5] H. Choi, J. Jeong, H.-B. Kim, S. Kim, B. Walker, G.-H. Kim, J. Y. Kim, *Nano Energy* **2014**, *7*, 80–85.

[6] G. E. Eperon, G. M. Paternò, R. J. Sutton, A. Zampetti, A. A. Haghighirad, F. Cacialli, H. J. Snaith, *J. Mater. Chem. A* **2015**, *3*, 19688–19695.

[7] Z. Li, F. Zhou, Q. Wang, L. Ding, Z. Jin, *Nano Energy* **2020**, *71*, 104634.

[8] X. Jia, C. Zuo, S. Tao, K. Sun, Y. Zhao, S. Yang, M. Cheng, M. Wang, Y. Yuan, J. Yang, F. Gao, G. Xing, Z. Wei, L. Zhang, H.-L. Yip, M. Liu, Q. Shen, L. Yin, L. Han, S. Liu, L. Wang, J. Luo, H. Tan, Z. Jin, L. Ding, *Sci. Bull.* **2019**, *64*, 1532–1539.

[9] A. Marronnier, G. Roma, S. Boyer-Richard, L. Pedesseau, J.-M. Jancu, Y. Bonnassieux, C. Katan, C. C. Stoumpos, M. G. Kanatzidis, J. Even, *ACS Nano* **2018**, *12*, 3477–3486.

[10] D. M. Trots, S. V. Myagkota, *J. Phys. Chem. Solids* **2008**, *69*, 2520–2526.

[11] R. J. Sutton, M. R. Filip, A. A. Haghighirad, N. Sakai, B. Wenger, F. Giustino, H. J. Snaith, *ACS Energy Lett.* **2018**, *3*, 1787–1794.

[12] W. Ke, I. Spanopoulos, C. C. Stoumpos, M. G. Kanatzidis, *Nat. Commun.* **2018**, *9*, 4785.

[13] J. A. Steele, H. Jin, I. Dovgaliuk, R. F. Berger, T. Braeckevelt, H. Yuan, C. Martin, E. Solano, K. Lejaeghere, S. M. J. Rogge, C. Notebaert, W. Vandezande, K. P. F. Janssen, B. Goderis, E. Debroye, Y.-K. Wang, Y. Dong, D. Ma, M. Saidaminov, H. Tan, Z. Lu, V. Dyadkin, D. Chernyshov, V. Van Speybroeck, E. H. Sargent, J. Hofkens, M. B. J. Roeffaers, *Science* **2019**, *365*, 679–684.

[14] H. Näsström, P. Becker, J. A. Márquez, O. Shargaieva, R. Mainz, E. Unger, T. Unold, *J. Mater. Chem. A* **2020**, *8*, 22626–22631.

[15] X. Yang, H. Yang, X. Hu, W. Li, Z. Fang, K. Zhang, R. Huang, J. Li, Z. Yang, Y. Song, *J. Mater. Chem. A* **2020**, *8*, 5308–5314.

[16] J. Wang, L. Cheng, Z. Qian, G. Ren, J. Wu, H. Zhang, *J. Mater. Chem. A* **2020**, *9*, 25336–25344.

[17] A. Shpatz Dayan, B.-E. Cohen, S. Aharon, C. Tenailleau, M. Wierzbowska, L. Etgar, *Chem. Mater.* **2018**, *30*, 8017–8024.

[18] K. Wang, Z. Li, F. Zhou, H. Wang, H. Bian, H. Zhang, Q. Wang, Z. Jin, L. Ding, S. (Frank) Liu, *Adv. Energy Mater.* **2019**, *9*, 1902529.

[19] C. C. Stoumpos, C. M. M. Soe, H. Tsai, W. Nie, J.-C. Blancon, D. H. Cao, F. Liu, B. Traoré, C. Katan, J. Even, A. D. Mohite, M. G. Kanatzidis, *Chem* **2017**, *2*, 427–440.

[20] Y. Shang, Z. Fang, W. Hu, C. Zuo, B. Li, X. Li, M. Wang, L. Ding, S. Yang, *J. Semicond.* **2021**, *42*, 050501.

[21] J. Li, Q. Yu, Y. He, C. C. Stoumpos, G. Niu, G. G. Trimarchi, H. Guo, G. Dong, D. Wang, L. Wang, M. G. Kanatzidis, *J. Am. Chem. Soc.* **2018**, *140*, 11085–11090.

[22] E. Breniaux, E. J. Marin-Bernardez, E. Gallet, P. Dufour, C. Tenailleau, *Mater. Chem. Phys.* **2020**, *247*, 122870.

[23] Z. Li, X. Liu, J. Xu, S. Yang, H. Zhao, H. Huang, S. F. Liu, J. Yao, *J. Phys. Chem. Lett.* **2020**, *11*, 4138–4146.

[24] Z. Li, X. Liu, J. Xu, S. Yang, H. Zhao, H. Huang, J. Yao, *J. Mater. Chem. C* **2020**, *8*, 6977,6987.

[25] S. Yang, W. Liu, Y. Han, Z. Liu, W. Zhao, C. Duan, Y. Che, H. Gu, Y. Li, S. (Frank) Liu, *Adv. Energy Mater.* **2020**, *10*, 2002882.

[26] H. Zhao, Y. Fu, Z. Li, S. Yang, B. Xu, X. Liu, J. Xu, S. Liu, J. Yao, *J. Mater. Chem. A* **2021**, *9*, 4922–4932.

[27] J. Xia, C. Liang, S. Mei, H. Gu, B. He, Z. Zhang, T. Liu, K. Wang, S. Wang, S. Chen, Y. Cai, G. Xing, *J. Mater. Chem. A* **2021**, *9*, 2919–2927.

[28] C. A. R. Perini, A. R. Pininti, S. Martani, P. Topolovsek, A. Perego, D. Cortecchia, A. Petrozza, M. Caironi, *J. Mater. Chem. A* **2020**, *8*, 25283–25289.

[29] G. Niu, H. Yu, J. Li, D. Wang, L. Wang, *Nano Energy* **2016**, *27*, 87–94.

[30] G. Kim, H. Min, K. S. Lee, D. Y. Lee, S. M. Yoon, S. I. Seok, *Science* **2020**, *370*, 108–112.

[31] Y. Yang, C. Liu, O. A. Syzgantseva, M. A. Syzgantseva, S. Ma, Y. Ding, M. Cai, X. Liu, S. Dai, M. K. Nazeeruddin, *Adv. Energy Mater.* **2021**, *11*, 2002966.

[32] Y. Zheng, X. Yang, R. Su, P. Wu, Q. Gong, R. Zhu, *Adv. Funct. Mater.* **2020**, *30*, 2000457.

[33] J. He, J. Liu, Y. Hou, Y. Wang, S. Yang, H. G. Yang, *Nat. Commun.* **2020**, *11*, 4237.

[34] F. Zheng, C. Zuo, M. Niu, C. Zhou, S. J. Bradley, C. R. Hall, W. Xu, X. Wen, X. Hao, M. Gao, T. A. Smith, K. P. Ghiggino, *ACS Appl. Mater. Interfaces* **2020**, *12*, 25980–25990.

[35] M. Kim, G.-H. Kim, T. K. Lee, I. W. Choi, H. W. Choi, Y. Jo, Y. J. Yoon, J. W. Kim, J. Lee, D. Huh, H. Lee, S. K. Kwak, J. Y. Kim, D. S. Kim, *Joule* **2019**, *3*, 2179–2192.

[36] S. You, X. Xi, X. Zhang, H. Wang, P. Gao, X. Ma, S. Bi, J. Zhang, H. Zhou, Z. Wei, *J. Mater. Chem. A* **2020**, *8*, 17756–17764.

[37] M. M. Tavakoli, P. Yadav, D. Prochowicz, M. Sponseller, A. Osherov, V. Bulović, J. Kong, *Adv. Energy Mater.* **2019**, *9*, 1803587.

[38] H. Hu, M. Singh, X. Wan, J. Tang, C.-W. Chu, G. Li, *J. Mater. Chem. A* **2020**, *8*, 1578–1603.

[39] A. Vailionis, H. Boschker, Z. Liao, J. R. A. Smit, G. Rijnders, M. Huijben, G. Koster, *Appl. Phys. Lett.* **2014**, *105*, 131906.

[40] M. Kepenekian, B. Traore, J.-C. Blancon, L. Pedesseau, H. Tsai, W. Nie, C. C. Stoumpos, M. G. Kanatzidis, J. Even, A. D. Mohite, S. Tretiak, C. Katan, *Nano Lett.* **2018**, *18*, 5603–5609.

[41] I. Mesquita, L. Andrade, A. Mendes, *Sol. Energy* **2020**, *199*, 474–483.

[42] C. Zhu, X. Niu, Y. Fu, N. Li, C. Hu, Y. Chen, X. He, G. Na, P. Liu, H. Zai, Y. Ge, Y. Lu, X. Ke, Y. Bai, S. Yang, P. Chen, Y. Li, M. Sui, L. Zhang, H. Zhou, Q. Chen, *Nat. Commun.* **2019**, *10*, 815.

[43] H.-S. Kim, N.-G. Park, *NPG Asia Mater.* **2020**, *12*, 1–14.

[44] J.-W. Lee, S. Tan, T.-H. Han, R. Wang, L. Zhang, C. Park, M. Yoon, C. Choi, M. Xu, M. E. Liao, S.-J. Lee, S. Nuryyeva, C. Zhu, K. Huynh, M. S. Goorsky, Y. Huang, X. Pan, Y. Yang, *Nat. Commun.* **2020**, *11*, 5514.

[45] D.-J. Xue, Y. Hou, S.-C. Liu, M. Wei, B. Chen, Z. Huang, Z. Li, B. Sun, A. H. Proppe, Y. Dong, M. I. Saidaminov, S. O. Kelley, J.-S. Hu, E. H. Sargent, *Nat. Commun.* **2020**, *11*, 1514.

[46] F. Ke, C. Wang, C. Jia, N. R. Wolf, J. Yan, S. Niu, T. P. Devereaux, H. I. Karunadasa, W. L. Mao, Y. Lin, *Nat. Commun.* **2021**, *12*, 461.

[47] Y. Cao, G. Qi, C. Liu, L. Wang, Z. Ma, K. Wang, F. Du, G. Xiao, B. Zou, *J. Phys. Chem. C* **2018**, *122*, 9332–9338.

[48] Y. Dong, K. Huang, J. Yang, J. Chang, J. Zhang, Y. Yang, *Nano Select* **2021**, *2*, 932–938.

[49] J. K. Nam, M. S. Jung, S. U. Chai, Y. J. Choi, D. Kim, J. H. Park, *J. Phys. Chem. Lett.* **2017**, *8*, 2936–2940.

[50] M. Afsari, A. Boochani, M. Hantezadeh, *Optik* **2016**, *127*, 11433–11443.

[51] T. J. Jacobsson, L. J. Schwan, M. Ottosson, A. Hagfeldt, T. Edvinsson, *Inorg. Chem.* **2015**, *54*, 10678–10685.

[52] J. A. Thornton, D. W. Hoffman, *Thin Solid Films* **1989**, *171*, 5–31.

[53] W. Hui, Y. Xu, F. Xia, H. Lu, B. Li, L. Chao, T. Niu, B. Du, H. Du, X. Ran, Y. Yang, Y. Xia, X. Gao, Y. Chen, W. Huang, *Nano Energy* **2020**, *73*, 104803.

[54] J. V. Patil, S. S. Mali, C. K. Hong, *J. Energy Chem.* **2021**, *62*, 451–458.

[55] T. Ozturk, E. Akman, A. E. Shalan, S. Akin, *Nano Energy* **2021**, *87*, 106157.

[56] W. Xiang, Z. Wang, D. J. Kubicki, X. Wang, W. Tress, J. Luo, J. Zhang, A. Hofstetter, L. Zhang, L. Emsley, M. Grätzel, A. Hagfeldt, *Nat. Commun.* **2019**, *10*, 4689.

[57] A. Le Bail, H. Duroy, J. L. Fourquet, *MRS Bull.* **1988**, *23*, 447–452.